

# Willis coupling-induced acoustic radiation force and torque reversal

Shahrokh Sepehrirahnama,<sup>1,\*</sup> Sebastian Oberst,<sup>1,†</sup> Yan Kei Chiang,<sup>2,‡</sup> and David A. Powell<sup>2</sup>

<sup>1</sup>Centre for Audio, Acoustics and Vibration, University of Technology Sydney, Sydney, Australia

<sup>2</sup>School of Engineering and Information Technology, University of New South Wales, Canberra, Australia

(Dated: October 5, 2021)

Acoustic meta-atoms serve as the building blocks of metamaterials, with linear properties designed to achieve functions such as beam steering, cloaking and focusing. They have also been used to shape the characteristics of incident acoustic fields, which led to the manipulation of acoustic radiation force and torque for development of acoustic tweezers with improved spatial resolution. However, acoustic radiation force and torque also depend on the shape of the object, which strongly affects its scattering properties. We show that by designing linear properties of an object using metamaterial concepts, the nonlinear acoustic effects of radiation force and torque can be controlled. Trapped objects are typically small compared to the wavelength, and are described as particles, inducing monopole and dipole scattering. We extend such models to a polarizability tensor including Willis coupling terms, as a measure of asymmetry, capturing the significance of geometrical features. We apply our model to a three-dimensional, sub-wavelength meta-atom with maximal Willis coupling, demonstrating that the force and the torque can be reversed relative to an equivalent symmetrical particle in acoustophoretic applications. By considering shape asymmetry in the acoustic radiation force and torque, Gorkov's fundamental theory of acoustophoresis is thereby extended. Asymmetrical shapes influence the acoustic fields by shifting the stable trapping location, highlighting a potential for tunable, shape-dependent particle sorting.

Keywords: Willis Coupling, Acoustic Radiation Force, Acoustic Radiation Torque, Bianisotropy, metamaterials, Ultrasound

Acoustic radiation force and radiation torque are the physical quantities underlying acoustophoresis - the manipulation of sub-wavelength objects by an incident acoustic field [1–8]. Applications such as ultrasonic sorting, separation and levitation have been developed by applying force and torque to objects such as biological cells [7, 9–15]. Considering their magnitude relative to gravitational force and fluid drag, acoustic radiation force and torque are most suitable for practical manipulation of sub-wavelength objects, with sizes ranging from sub-micrometers to a few millimeters [8, 16–24]. Existing theoretical derivations of the acoustic radiation force and radiation torque use simple shapes such as spheres, spheroids, cylinders and disks, leading to simple expressions which show the influence of the object's volume, material and aspect ratio [25–31]. This simplification of the exterior shape neglects the effect of asymmetry, which is a potential degree of freedom to tune acoustophoretic processes, for example targeted and simultaneous trapping and manipulation of a heterogeneous mixture of sub-wavelength objects in an ultrasonic standing wave, as illustrated in Fig. 1. From Gorkov's theory of acoustophoresis for small structures and shape asymmetry neglected, objects are found to be trapped at pressure or velocity nodes, cf. Fig. 1(a), depending on their dominant scattering mode [20, 32]. However, when shape asymmetry is accounted for, the effect on trapping locations is unknown so that these stable acoustic traps may shift away from the pressure node, as shown in Fig. 1(b).

Considering the key role of acoustic radiation force and torque in the ultrasonic range, it is important to capture the effects of geometric asymmetry on these force and torque fields. Recent advances in asymmetric metamaterials indicate growing interest in designs based on engineered geometries, either as a material of a single meta-atom for beam steering [33–36] or used as a material made of an array of meta-gratings

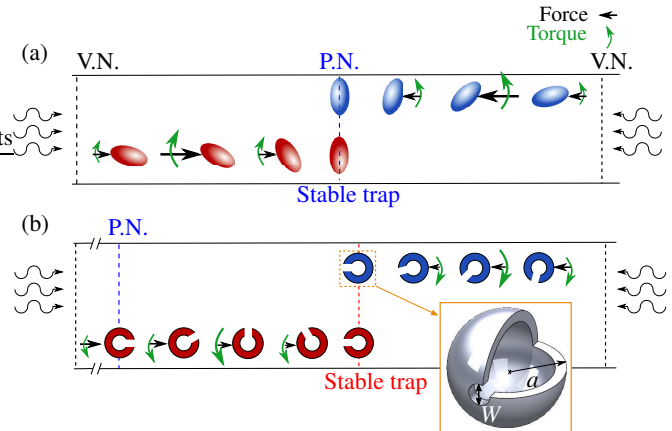


FIG. 1: Acoustic trapping of objects with (a) zero and (b) non-zero Willis Coupling, corresponding to the symmetric and asymmetric shapes, respectively. The asymmetry in the shape affects the locations of an acoustic trap and the stable orientation of the objects in it. Inset: The proposed meta-atom based on an internal Helmholtz resonator is a possible design to achieve such non-conventional acoustic trapping. PN and VN stand for Pressure Node and Velocity Node of an incident acoustic field. Stable trap refers to the location of zero radiation force with negative force gradient.

for beam splitting [37]. Such asymmetric shapes are characterised by Willis coupling, which describes the monopole and dipole moments induced by the incident velocity and pressure fields, respectively [38]. This coupling has a theoretical upper limit and approaches zero as the object approaches a mirror-symmetric configuration [33]. By geometrical modifications such as adding protruding holes and internal cavities, the Willis coupling and its effect on the acoustic field can be

controlled [36, 38–40]. In particular, a two-dimensional C-shaped Helmholtz resonator can achieve the maximum Willis coupling near its resonance, or other arbitrary values by having multiple apertures of different sizes [35].

To investigate the influence of Willis coupling on the acoustic radiation force and torque, we consider a three-dimensional version of the Helmholtz resonator based meta-atom, as illustrated in Fig. 1(b). Since it is aimed for the ultrasonic range, narrow and long passages are avoided due to their role in unwanted thermo-viscous losses [36]. The 3D meta-atom has an internal cavity, occupying 60% of the volume, and one aperture of width  $W = 0.2a$  with  $a$  being the outer radius of the spherical shell, which acts as the normalization parameter, cf. Fig. 1(b). These parameters are tuned to achieve maximum Willis coupling along a single axis [35]. The values of  $a$  are varied from  $0.01\lambda$  to  $0.16\lambda$  to focus on the limit of  $ka \ll 1$ . We assume that the meta-atom behaves as a sound-hard and immovable object in the acoustic domain. This assumption allows comparison with existing radiation force theory, which predicts, in the case of a plane standing wave, sound-hard immovable spheres or spheroids are always pushed towards the pressure nodes. These are the stable acoustic trap locations with zero force and negative force gradient, as shown schematically in Fig. 1. For the analysis of radiation torque a sound-hard immovable prolate spheroid of sub-wavelength size is used as a reference [41], to avoid the peaks occurring for  $ka > 1$ .

The incident field is taken as a plane standing wave with  $p_i = P_a \cos(kz)e^{-j\omega t}$ , and the meta-atom is represented by its monopole-dipole polarizability tensor  $\boldsymbol{\alpha} = \begin{bmatrix} \alpha_{pp} & \boldsymbol{\alpha}_{pv}^T \\ \boldsymbol{\alpha}_{vp} & \alpha_{vv} \end{bmatrix}$ . The acoustic radiation force and torque are derived as the sum of symmetric and asymmetric terms [42],  $\mathbf{F} = \mathbf{F}_{\text{sym}} + \mathbf{F}_{\text{asym}}$  and  $\mathbf{T} = \mathbf{T}_{\text{sym}} + \mathbf{T}_{\text{asym}}$  with

$$\mathbf{F}_{\text{sym}} = \frac{kE_i}{\rho_f} \left( \frac{\Re[\alpha_{pp}]}{\kappa_f} \mathbf{e}_z - kc_f \Im[\boldsymbol{\alpha}_{vv} \mathbf{e}_z] \cdot \mathbf{e}_z \mathbf{e}_z \right) \sin(2kz), \quad (1)$$

$$\mathbf{F}_{\text{asym}} = \frac{kE_i}{\rho_f} c_f \Im[2\boldsymbol{\alpha}_{pv} \cdot (\mathbf{e}_z \mathbf{e}_z)] \cos(2kz),$$

$$\mathbf{T}_{\text{sym}} = -\frac{kE_i}{\rho_f} c_f \Im[2\boldsymbol{\alpha}_{vv} \mathbf{e}_z] \times \mathbf{e}_z \sin^2(kz), \quad (2)$$

$$\mathbf{T}_{\text{asym}} = \frac{kE_i}{\rho_f} \left( \frac{1}{\kappa_f} \Re[\boldsymbol{\alpha}_{vp}] \times \mathbf{e}_z \right) \sin(2kz),$$

where subscript sym denotes the partial force and torque associated with direct-polarization coefficients  $\alpha_{pp}$  and  $\boldsymbol{\alpha}_{vv}$ , known from Gorkov's theory. The terms with the subscript asym are induced by the Willis coupling coefficients  $\boldsymbol{\alpha}_{pv}$  and  $\boldsymbol{\alpha}_{vp}$  which obey  $\boldsymbol{\alpha}_{pv} = j\omega \rho_f \boldsymbol{\alpha}_{vp}^T$  for reciprocal media. These asymmetry-induced terms show the direct correlation between shape asymmetry and the two fields of acoustic radiation force and radiation torque. This is illustrated in Fig. 1(b), with objects exhibiting strong Willis coupling being trapped in a different location than their symmetric counterparts, cf. Fig. 1(a).

An incident pressure field of 10 mm wavelength in air is considered, with the speed of sound  $c_f = 343.140 \text{ ms}^{-1}$  and mean density  $\rho_f = 1.204 \text{ kg m}^{-3}$ . The acoustic radiation force and torque values are normalized as  $\mathbf{Q} = \mathbf{F}/(E_i \pi a^2)$  and  $\mathbf{Z} = \mathbf{T}/(E_i \pi a^3)$ , which are commonly referred to as force contrast factor and torque contrast factor, respectively. The energy density of the incident wave is  $E_i = p_i^2/(4\rho_f c_f^2)$ .

The non-zero coefficients of the normalized polarizability tensor of the meta-atom are shown in Fig. 2(a), with respect to the size index  $ka$ . The results are scaled by  $6\pi/(c_f^2 k^3)$ , which is the maximum permissible value of normalized Willis coupling coefficients [33]. Real and imaginary parts of polarizability coefficients are provided in Fig. (2) of the Supplementary Notes. A resonant peak is found at  $ka \approx 0.17$ , and a trough, indicating a zero root, is observed for  $\alpha_{pp}$  at  $ka \approx 0.12$ , implying no contribution from incident pressure field to the monopole moment. The resonant peak is only observed in the polarizability coefficients that are associated with the aperture facing the  $z$ -direction. These two effects originate from the internal cavity, changing the scattering strength of the monopole mode. By using Eqs. (1) and (2), the radiation force and torque are obtained directly from the polarizability coefficients. The magnitude of these radiation force and torque with respect to size index are shown in Fig. 2(b) and Fig. 2(c), respectively. The meta-atom is oriented at a fixed angle of  $-\pi/4$  with respect to the positive wave direction  $\hat{z}$ , as shown in the inset of Fig. 2(c), to ensure non-zero torque. The torque acts in the  $y$ -direction, and the force components in the  $x$ - and  $z$ -directions are equal. Equation (1) is verified by comparing with the force obtained by direct integration of radiation stresses over a fictitious surface of radius  $4\lambda$  enclosing the meta-atom [2, 27, 42]. The contributions of the direct and Willis-coupling partial forces are plotted in Fig. 2(b). The local minimum in the  $Q_{\text{sym}}$  at  $ka \approx 0.16$  emerges as a result of the zero root of  $\alpha_{pp}$  at  $ka_{\text{root}} \approx 0.12$ . This is due to  $F_{\text{sym}}$  being determined by  $\alpha_{pp}$  as well as  $\alpha_{vv}^{zz}$ , which is non-zero within this entire range of  $ka$ . The radiation torque exhibits no local minimum since it is independent of the monopole scattering term  $\alpha_{pp}$ , as shown in Eq. (2). The orientation of the object with respect to the wave propagation direction changes the acoustic radiation force and radiation torque, as shown analytically in Section 1 of the Supplementary Notes.

Fig. 2(d) and Fig. 2(e) show the acoustic radiation force and radiation torque with respect to position  $z$  and incidence angle  $\theta$  for the specific case of  $ka_{(II)} \approx 0.16$ . This frequency is chosen since the radiation force is dominated by the Willis-coupling partial force. The direction of the force and torque are indicated by the arrows in each region. In contrast to the case for symmetric objects, the radiation force is no longer zero at the pressure node location,  $z/\lambda = 0.25$ ; implying a significant shift in the stable trapping point due to shape asymmetry. It is also observed that the force depends on angle  $\theta$ , meaning that the stable acoustic trap occurs where both the force and torque are zero, corresponding to the intersection of the zero contours in Fig. 2(d) and (e). These zero force and torque contours are plotted in Fig. 2(f), leading to four inter-

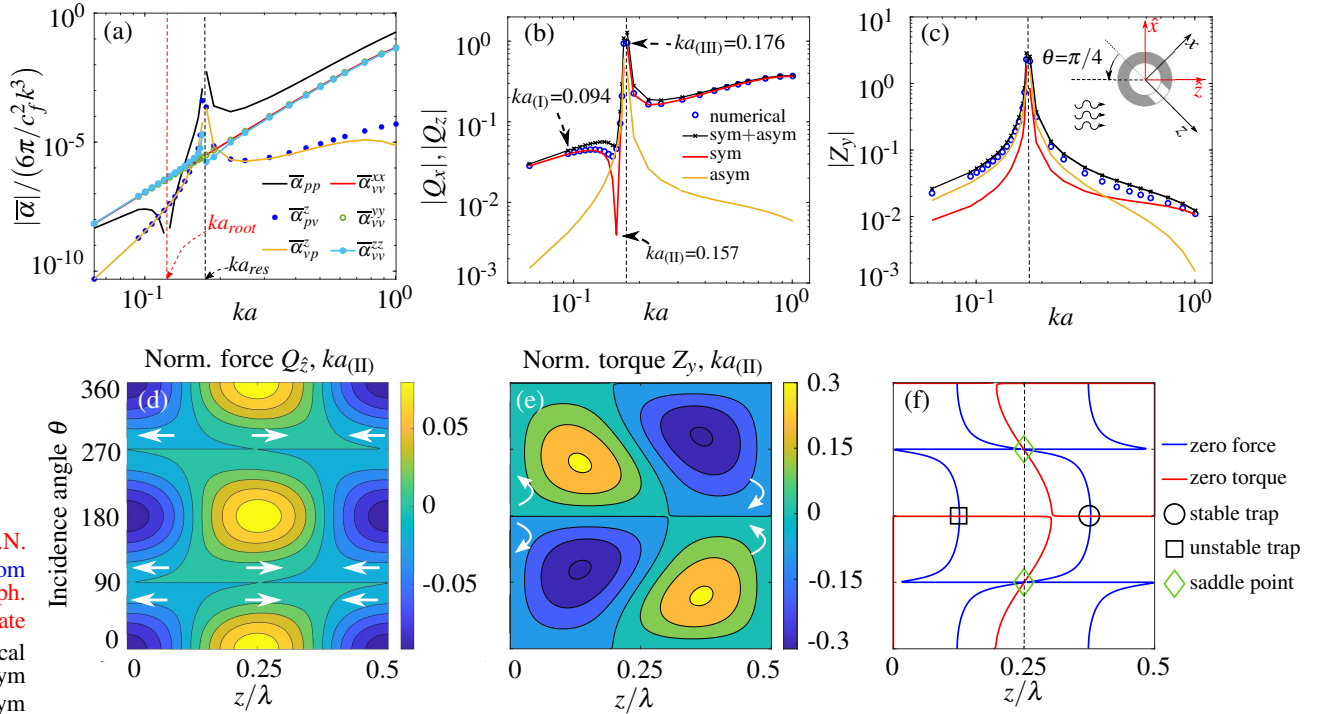


FIG. 2: Panel (a) shows the absolute value of the non-zero and normalized polarizability coefficients for the 3D meta-atom. Normalized radiation force and torque with respect to the size index  $ka$  for the  $\theta = \pi/4$  incidence angle are shown in panels (b) and (c), respectively. The magnitude of these quantities are denoted by  $|\mathbf{Q}|$  and  $|\mathbf{Z}|$ . Panels (d) and (e) are the normalized force and torque, respectively, for the case of  $ka_{(II)} = 0.157$  with respect to position and incidence angle. Panel (f) shows the loci of zero force and zero torque and locations of saddle points, unstable and stable acoustic trap.

section points. Of these four points, only one is stable (circle marker), since both the force and torque gradients are negative. Analysis of the force and torque gradients reveals that the other three points are unstable. For the point marked by a square, any perturbation of position or torque will grow, leading the particle to escape. The points marked with diamonds are saddle points, where particular combinations of torque and force perturbation will lead to the particle escaping.

We now investigate the force and torque distributions at different positions within the standing wave  $z/\lambda$ , as shown in Fig. 3. We consider three different frequency regimes, to show the drastic impact of the resonance on the trapping location. In panels (a) and (d) we show the results for  $ka_{(I)}$ , corresponding to a low frequency limit where the Willis coupling is much smaller than the direct polarizability terms. As expected, the Willis-coupling partial force (asym in Fig. 3(a)) is negligible compared to the direct polarization contribution,  $F_{\text{sym}}$  (sym in Fig. 3(a)). Considering an equivalent sphere,  $F_{\text{sym}}$  predicts a stable trap at the pressure node where the force is zero with a negative gradient (Fig. 3(a)). This matches the classical prediction of spherical sound-hard particles being trapped at the pressure node in a plane standing wave [2, 16–18, 20, 32, 43]. However, the predicted acoustic trap determined by the sum of the two partial forces, shown by the solid blue line, is slightly shifted from the pressure node, as a result of the

Willis-coupling partial force being dominant in that region. The radiation torque result shown in Fig. 3(d) is compared against an equivalent prolate spheroid having the same diagonal polarizability coefficients as the meta-atom. We observe the Willis-coupling torque being dominant, resulting in an additional zero-torque location at  $z/\lambda \approx 0.21$ , unlike the prolate spheroid which only experiences zero-torque at the velocity nodes  $z = 0$  and  $z = \lambda/2$ .

In Fig. 3(b) and (e), we consider the frequency  $ka_{(II)} = 0.157$ , corresponding to a local minimum of the direct force term  $F_{\text{sym}}$ , so that the total radiation force is determined by the Willis-coupling contribution. This causes the stable trap to shift by  $z/\lambda = 0.125$ , which is a considerable distance away from the pressure node, where the equivalent sphere is trapped. This shift is so large, that it corresponds to the point where the symmetric contribution to the force is maximum - illustrating that asymmetric particles can show behavior directly contradicting the conventional Gorkov theory. Although  $F_{\text{sym}}$  is relatively small, we observe a direction reversal of the force vector in comparison to  $ka_{(I)}$ . Such force reversal is typically expected only for  $ka > 1$  [28, 41], due to the resonant modes of the outer fluid domain. However, our proposed meta-atom undergoes such force reversal due to the internal cavity acting as a Helmholtz resonator and the maximized Willis coupling associated with its single aperture. The

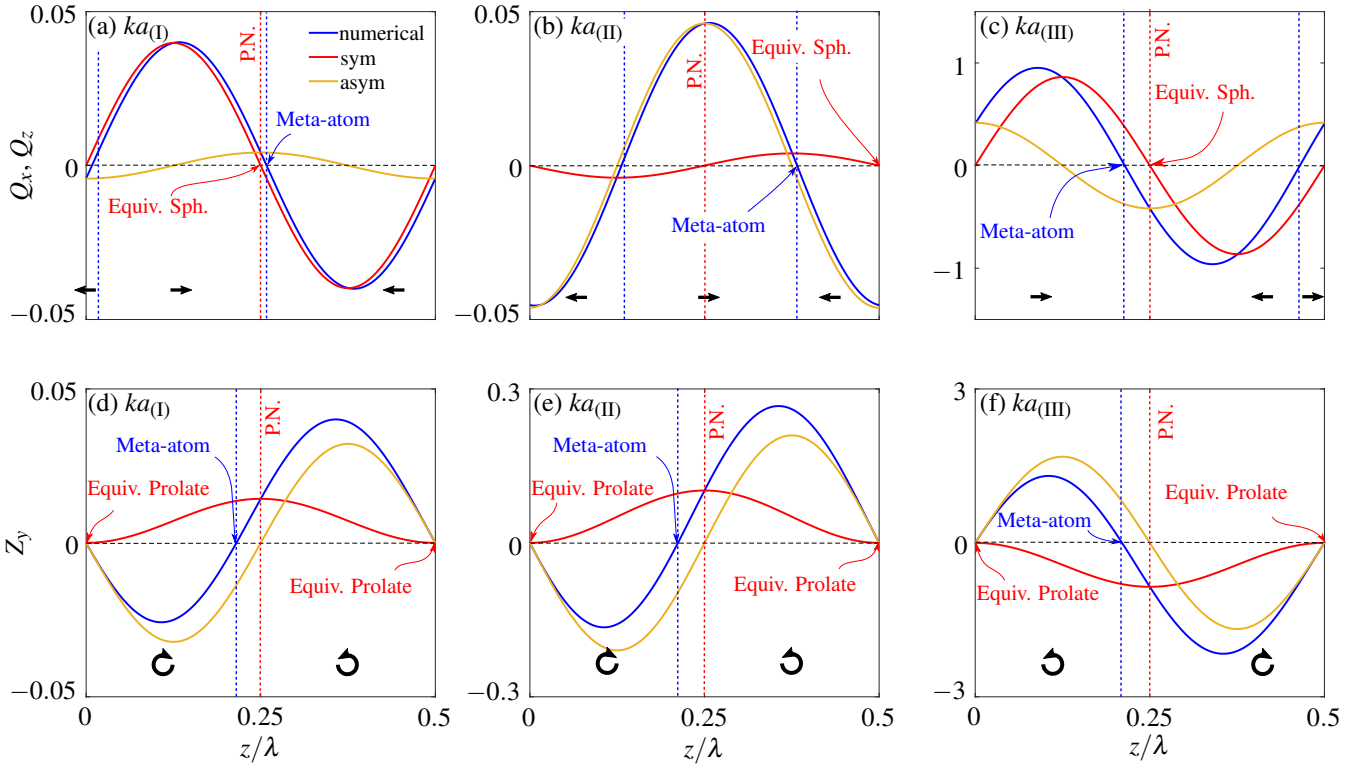


FIG. 3: Variations of the normalized radiation force, panels (a)-(c), and radiation torque, panels (d)-(f), over a half wave-length span between two velocity nodes of a plane standing wave in the  $z$  direction. The results are shown for three different  $ka$  values, indicated in Fig. 2(b).

torque is determined by the large contribution from the Willis-coupling partial torque, and the stable angular equilibrium occurs at a point further to the left of the pressure node than for  $ka_{(I)}$ .

Close to the resonance peak, at  $ka_{(III)}$ , the total radiation force and  $F_{\text{sym}}$  shown in Fig. 3(c) exhibit the same direction as predicted by Gorkov theory. We also observe a reversal of the Willis-coupling partial force  $F_{\text{asym}}$ , resulting in a large negative shift of more than  $10a$  in the location of the stable trap relative to the case for  $ka_{(II)}$  (Fig. 2(b)). The reversal of the torque shown in Fig. 3(f) indicates its tendency to orient the aperture in the opposite direction to that obtained for  $ka_{(I)}$  and  $ka_{(II)}$ . The stable angular equilibrium is still found at  $z/\lambda \approx 0.21$ , due to the direction reversal of both partial torques.

Our results provide physical insight into the relationship between shape asymmetry and force and torque reversal, which we show here are also possible for  $ka < 1$ . Willis coupling in general describes structure-inherent asymmetry, which can be related to geometrical anomalies of a trapped object. In addition to anomalous scattering, meta-atoms with strong Willis coupling were shown to experience different acoustic radiation forces and radiation torques, indicating the potential to control these nonlinear acoustic phenomena through Willis coupling. Applications such as particle sorting, could be tuned

to process objects with similar shape features by generating traps at locations other than pressure/velocity nodes. Further, by maximizing Willis coupling by setting the ratio between wavelength and asymmetric feature size, single objects could be re-oriented this way. As these effects already take place within the sub-wavelength regime, target-specific ultrasound manipulation techniques for the control of biological cells or small tissue ensembles could be designed by mixing with meta-objects. This control of field quantities using metamaterial concepts for shape-dependent separation of heterogeneous suspension mixtures or adapting self-assembly processes with tailored acoustic beams is likely to provide a fresh approach to the field of acoustophoresis.

This research was supported by the Australian Research Council through Discovery Projects DP200101708 and DP200100358.

\* shahrokh.sepehrirhanama@uts.edu.au

† Also at School of Engineering and Information Technology, University of New South Wales, Canberra, Australia

‡ Also at Centre for Audio, Acoustics and Vibration, University of Technology Sydney, Sydney, Australia

[1] H. Bruus, *Lab on a Chip* **11**, 3742 (2011).

[2] H. Bruus, *Lab on a Chip* **12**, 1014 (2012).

[3] A. Lenshof, C. Magnusson, and T. Laurell, *Lab on a Chip* **12**, 1210 (2012).

[4] H. Bruus, *Lab on a Chip* **12**, 1578 (2012).

[5] J. Dual, P. Hahn, I. Leibacher, D. Möller, T. Schwarz, and J. Wang, *Lab on a Chip* **12**, 4010 (2012).

[6] M. Wiklund, R. Green, and M. Ohlin, *Lab on a Chip* **12**, 2438 (2012).

[7] D. Hartono, Y. Liu, P. L. Tan, X. Y. S. Then, L.-Y. L. Yung, and K.-M. Lim, *Lab on a Chip* **11**, 4072 (2011).

[8] A. R. Mohapatra, S. Sepehrirahnama, and K.-M. Lim, *Physical Review E* **97**, 053105 (2018).

[9] P. Augustsson, C. Magnusson, M. Nordin, H. Lilja, and T. Laurell, *Analytical chemistry* **84**, 7954 (2012).

[10] A. Bernassau, P. Glynne-Jones, F. Gesellchen, M. Riehle, M. Hill, and D. Cumming, *Ultrasonics* **54**, 268 (2014).

[11] M. Antfolk, C. Magnusson, P. Augustsson, H. Lilja, and T. Laurell, *Analytical chemistry* **87**, 9322 (2015).

[12] A. Marzo, S. A. Seah, B. W. Drinkwater, D. R. Sahoo, B. Long, and S. Subramanian, *Nature communications* **6**, 8661 (2015).

[13] F. B. Wijaya, A. R. Mohapatra, S. Sepehrirahnama, and K.-M. Lim, *Microfluidics and Nanofluidics* **20**, 69 (2016).

[14] A. Marzo and B. W. Drinkwater, *PNAS* **116**, 84 (2019).

[15] S. Polychronopoulos and G. Memoli, *Scientific reports* **10**, 1 (2020).

[16] L. V. King, *Proceedings of the Royal Society of London. Series A-Mathematical and Physical Sciences* **147**, 212 (1934).

[17] K. Yoshioka and Y. Kawasima, *Acta Acustica united with Acustica* **5**, 167 (1955).

[18] L. P. Gorkov, *Soviet Physics - Doklady* **6**, 773 (1962).

[19] A. A. Doinikov, *Journal of Fluid Mechanics* **267**, 1 (1994).

[20] M. Settnes and H. Bruus, *Physical Review E* **85**, 016327 (2012).

[21] G. T. Silva and H. Bruus, *Physical Review E* **90**, 063007 (2014).

[22] P. L. Marston, *The Journal of the Acoustical Society of America* **120**, 3518 (2006).

[23] F. Mitri, *Wave Motion* **57**, 231 (2015).

[24] A. Garcia-Sabaté, A. Castro, M. Hoyos, and R. González-Cinca, *The Journal of the Acoustical Society of America* **135**, 1056 (2014).

[25] A. A. Doinikov, *Proceedings of the Royal Society of London. Series A: Mathematical and Physical Sciences* **447**, 447 (1994).

[26] D. Foresti, M. Nabavi, and D. Poulikakos, *Journal of Fluid Mechanics* **709**, 581 (2012).

[27] F. B. Wijaya and K.-M. Lim, *Acta Acustica united with Acustica* **101**, 531 (2015).

[28] F. Mitri, *Journal of Applied Physics* **118**, 214903 (2015).

[29] W. Wei, D. B. Thiessen, and P. L. Marston, *The Journal of the Acoustical Society of America* **116**, 201 (2004).

[30] W. Xie and B. Wei, *Physical Review E* **70**, 046611 (2004).

[31] A. Garbin, I. Leibacher, P. Hahn, H. Le Ferrand, A. Studart, and J. Dual, *The Journal of the Acoustical Society of America* **138**, 2759 (2015).

[32] S. Sepehrirahnama and K.-M. Lim, *Physical Review E* **102**, 043307 (2020).

[33] L. Quan, Y. Ra'di, D. L. Sounas, and A. Alù, *Physical Review Letters* **120**, 254301 (2018).

[34] J. Jordaan, S. Punzet, A. Melnikov, A. Sanches, S. Oberst, S. Marburg, and D. A. Powell, *Applied Physics Letters* **113**, 224102 (2018).

[35] A. Melnikov, Y. K. Chiang, L. Quan, S. Oberst, A. Alù, S. Marburg, and D. Powell, *Nature communications* **10**, 1 (2019).

[36] Y. K. Chiang, S. Oberst, A. Melnikov, L. Quan, S. Marburg, A. Alù, and D. A. Powell, *Physical Review Applied* **13**, 064067 (2020).

[37] H. Ni, X. Fang, Z. Hou, Y. Li, and B. Assouar, *Physical Review B* **100**, 104104 (2019).

[38] C. F. Sieck, A. Alù, and M. R. Haberman, *Physical Review B* **96**, 104303 (2017).

[39] X. Su and A. N. Norris, *Physical Review B* **98**, 174305 (2018).

[40] A. Melnikov, M. Maeder, N. Friedrich, Y. Pozhanka, A. Wollmann, M. Scheffler, S. Oberst, D. Powell, and S. Marburg, *The Journal of the Acoustical Society of America* (2020).

[41] F. Mitri, *Ultrasonics* **49**, 794 (2009).

[42] S. Sepehrirahnama, S. Oberst, Y. Chiang, and D. Powell, *Arxiv* (2021).

[43] S. Sepehrirahnama and K.-M. Lim, *Microfluidics and Nanofluidics* **24**, 1 (2020).